THE JOURNAL OF PHYSICAL CHEMISTRY Letters

Letter

Cite This: J. Phys. Chem. Lett. 2018, 9, 2433−2437

pubs.acs.org/JPCL

A Natively Monomeric Deubiquitinase UCH-L1 Forms Highly Dynamic but Defined Metastable Oligomeric Folding Intermediates

Yun-Tzai Cloud Lee[†,‡] and Shang-Te Danny Hsu*[,†,‡]

[†]Institute of Biological Chemistry, Academia Sinica, Taipei 11529, Taiwan

[‡]Institute of Biochemical Sciences, National Taiwan University, Taipei 10617, Taiwan

Supporting Information

ABSTRACT: Oligomerization of misfolded protein species is implicated in many human disorders. Here we showed by size-exclusion chromatography-coupled multiangle light scattering (SEC-MALS) and small-angle X-ray scattering (SEC-SAXS) that urea-induced folding intermediate of human ubiquitin C-terminal hydrolase, UCH-L1, can form well-defined dimers and tetramers under denaturing conditions despite being highly disordered. Introduction of a Parkinson disease-associated mutation, I93M, resulted in increased aggregation propensity and formation of irreversible precipitants in the presence of a moderate amount of urea. Since UCH-L1 exhibits highly populated partially unfolded forms under native conditions that resemble urea-induced folding intermediates, it is likely that these metastable dimers and tetramers can form under physiological conditions. Our findings highlighted the unique strength of integrated SEC-MALS/SAXS in quantitative analyses of the structure and dynamics of oligomeric folding intermediates that enabled us to extract information that is inaccessible to conventional biophysical techniques.

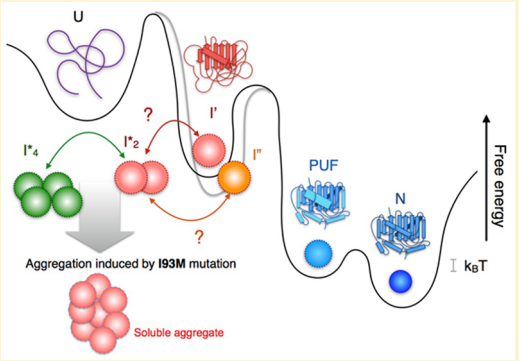

Protein folding often involves the formation of folding intermediates that contain partially unfolded forms (PUFs), which tend to self-associate leading to accumulation of aggregation-prone toxic oligomers and eventually causing debilitating human disorders such as Alzheimer's disease and Parkinson's disease (PD).[1,2] While protein misfolding is a common feature shared among many neurodegenerative diseases and non-neuropathic systemic amyloidosis, detailed structural features of the early oligomers of the pathogenic proteins vary significantly.[3] Continuous efforts have been devoted into gaining mechanistic insights of protein misfolding and amyloid formation.[4,5] In many cases, conformational rearrangements within the early oligomers are found to be closely associated with their seeding effects.[6,7] Extensive studies have been reported to address the question of the exact number of monomers within different types of early oligomers and how they subsequently form proto-filaments and the eventual amyloid fibrils.[8,9]

Human ubiquitin carboxyl-terminal hydrolase, UCH-L1 (also known as PGP9.5 or PARK5), is a deubiquitinase that is highly expressed in neurons.[10] It is a potential risk factor in PD and is frequently found together with α-synuclein inclusions in Lewy bodies, the hallmark of PD. A familial isoleucine to methionine mutation at residue position 93 in UCH-L1 (I93M) has been identified in one German family with late onset autosomal dominant PD leading to its association with increased risk of PD.[11] This mutation is located adjacent to the catalytic site, which could be responsible for the reduced DUB activity,[11] increased aggregation propensity,[12] and aberrant interactions with cellular factors such as molecular chaperones, e.g., Hsc70 and Hsp90, with the potential to interfere with chaperone-mediated autophagy and accumulation of α-synuclein aggregates.[13] Post-translational modifications by reactive metabolite can cause similar aggregation propensity.[14−17]

Using solution-state NMR spectroscopy, we observed significant structural perturbations far beyond the I93M mutation sites evidenced by significant chemical shift perturbations[18] despite the indistinguishable crystal structures between UCH-L1 wild type (WT) and the I93M variant.[19,20] We further demonstrated that the I93M mutation significantly reduces the folding stability and accelerates the urea-induced unfolding kinetics of UCH-L1.[18] Recently, we identified two obligatory and distinct kinetic folding intermediates being populated along each of the two parallel folding pathways connecting the native and denatured states of UCH-L1.[21] Furthermore, native and pulsed-labeling NMR hydrogen−deuterium exchange (HDX) analyses revealed the presence of highly populated PUFs of UCH-L1 that share the same structural features with chemically induced folding intermediates.[21] Although UCH-L1 is monomeric in solution under the native condition, we observed significant protein concentration dependency in the equilibrium intermediate population induced by urea (Figure S1) that was overlooked in previous

Received: March 15, 2018
Accepted: April 24, 2018
Published: April 24, 2018

Downloaded via SYNCHROTRON RADIATION RESEARCH on January 21, 2019 at 03:47:45 (UTC).
See https://pubs.acs.org/sharingguidelines for options on how to legitimately share published articles.

ACS Publications © 2018 American Chemical Society

DOI: 10.1021/acs.jpclett.8b00815
J. Phys. Chem. Lett. 2018, 9, 2433−2437

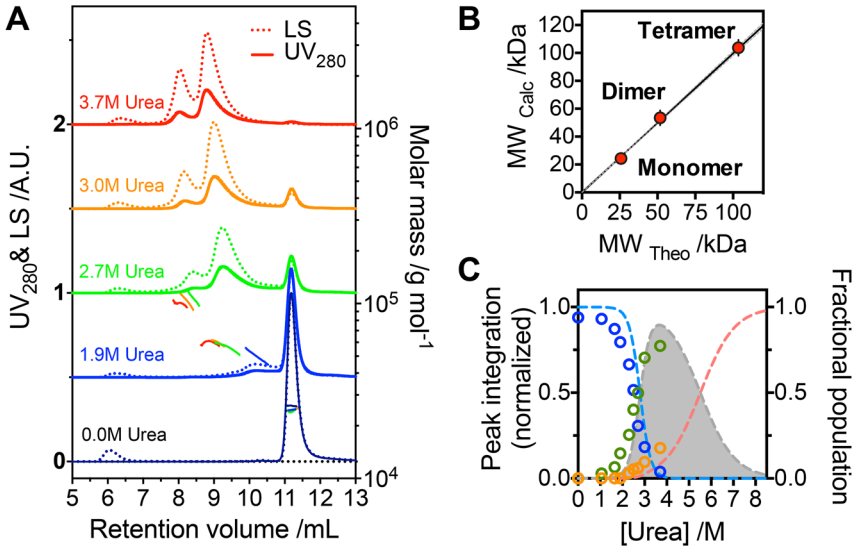

Figure 1. Urea-induced oligomerization of UCH-L1. (A) SEC-MALS profiles of UCH-L1 in the presence of different urea concentrations as indicated. The calculated MWs are indicated at the peak positions. The dotted line and solid line indicate light scattering (LS) and UV absorption at 280 nm (UV_{280}). (B) Correlation between calculated and theoretical MWs (MW_{Calc} and MW_{Theo}) associated with the individual elution peaks in (A). (C) Elution peak integrals corresponding to monomer (open blue), dimer (open green), and tetramer (open orange) as a function of urea concentration. Intrinsic fluorescence-derived native, intermediate, and denatured state populations (these populations were derived from an equilibrium three-state folding model at a protein concentration of ca. 40 μM as shown in Figure S1) are shown as a dash blue line, shaded gray area, and dashed red line, respectively.

equilibrium analyses.[18,21] This result implies that the chemically induced folding intermediate of UCH-L1 is oligomeric.

To further characterize the nature of these oligomeric folding intermediates, we carried out analytical size-exclusion chromatography-coupled multiangle static light scattering (SEC-MALS) to determine the oligomeric states of UCH-L1 in the presence of varying amounts of urea (Figure 1A). The results revealed the emergence of a well-defined dimeric UCH-L1 elution peak in the presence of 1.9 M urea and subsequent emergence of tetrameric UCH-L1 elution peak on increasing urea concentration, ranging from 2.7 to 3.7 M urea. The molecular weights (MWs) of the dimer and tetramer elution peaks derived from SEC-MALS were a perfect match with the theoretical values (Figure 1B and Table S1 in the Supporting Information). Furthermore, the populations of the different oligomeric states as a function of urea concentration agreed well with the three-state population distributions derived from intrinsic fluorescence (Figure 1C and Supporting Information). In bulk fluorescence measurements, the optical contributions of different oligomeric states to the intermediate population could not be resolved. Therefore, the intermediate population (gray area in Figure 1c) corresponded to a lump sum of different oligomeric forms. Time-dependent SEC-MALS analysis indicated that UCH-L1 fully converted into dimer when mixed with 3.5 M urea within instrument dead time of 2.5 min; subsequent emergence of tetrameric population was observed after 10 min and beyond, indicating a sequential oligomerization process for the chemically induced folding intermediates (Figure S3).

Global fitting of the loss of dimeric population and the increase of tetrameric population of UCH-L1 at 3.5 M urea yielded a slow apparent rate of the tetramer formation (k_{app} = 0.022 ± 0.005 h^{-1}; Figure S3). Note that the kinetic analysis was carried out without considering the protein concentration dependency. Due to instrument limitation, SEC-MALS analysis was limited to urea concentration up to 4 M. To cover a wider range of urea concentrations, we applied chemical cross-linking using (bis[sulfosuccinimidyl] suberate (BS^3) in the presence of 0−8 M urea, followed by SDS-PAGE imaging analyses to quantify the amount of dimer and tetramer as a function of urea concentration. The results showed peak distributions of dimer and tetramer populations that were in general agreement with the intrinsic fluorescence-derived distributions, confirming the intrinsic oligomerization propensity of urea-induced folding intermediates of UCH-L1 (Figure S4).

SEC-MALS analysis of the PD-associated I93M variant of UCH-L1 showed a similar trend of oligomerization of urea-induced folding intermediates with a much more pronounced aggregation propensity (Figure 2A). In the presence of 1−2 M urea, higher oligomers were observed by SEC-MALS resulting in a continuum of MW distribution to the void volume with an apparent MW beyond one megadalton (Figure 2B). Prolonged overnight incubation under these conditions led to visible precipitates with significant turbidity that could be quantified by optical absorbance at 550 nm ($OD_{550\ nm}$; Figure 2C). The peak distribution of precipitating aggregates coincided with the emergence of intermediate population, consistent with the previously reported increased aggregation propensity caused by I93M mutation *in vitro* and *in vivo*.[13,14]

Collectively, our data suggested hierarchical formation of UCH-L1 oligomers upon urea-induced unfolding starting from a partially unfolded monomeric folding intermediate followed by the formation of dimers and tetramers (Figure S3). In the case of I93M, whose PUFs and folding intermediates may be different from that of the WT, exhibited a much higher aggregation propensity that could easily self-assemble into amorphous aggregates. To assess the structural features of these oligomers under non-native conditions, we carried out size exclusion chromatography-coupled small-angle X-ray scattering analysis (SEC-SAXS),[22,23] which has been applied to study protein folding and self-association under a variety of experimental conditions,[24−26] to deconvolute the scattering

DOI: 10.1021/acs.jpclett.8b00815
J. Phys. Chem. Lett. 2018, 9, 2433−2437

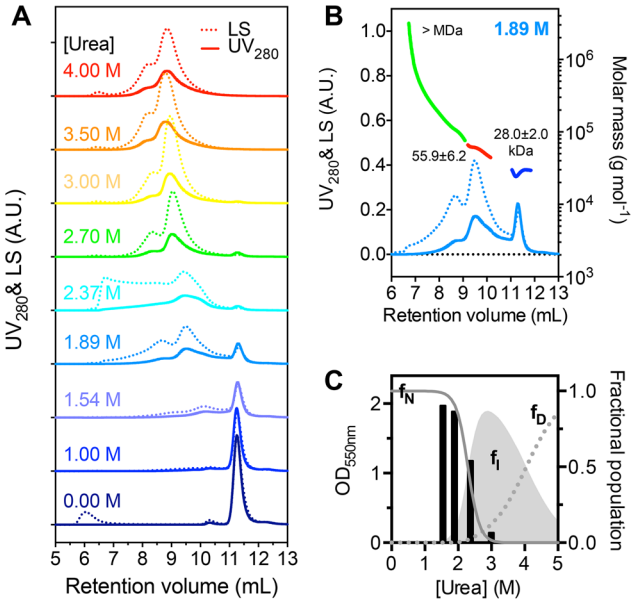

Figure 2. Increased aggregation propensity of PD-associated I93M variant. (A) SEC-MALS profiles of I93M in the presence of different urea concentrations as indicated. UV absorbance at 280 nm (UV_{280}) and light scattering intensity (LS) are shown in solid and dashed lines, respectively. (B) MW profiles of I93M variant in the presence of 1.89 M urea. The calculated MWs of monomer (blue), dimer (red) are indicated in kDa, and that of the large aggregate is shown in green down to the void volume (6 mL). (C) Sample turbidity (black bars) as a function of urea concentration and superimposed with the three-state fractional populations of I93M at a protein concentration of ca. 40 μM.

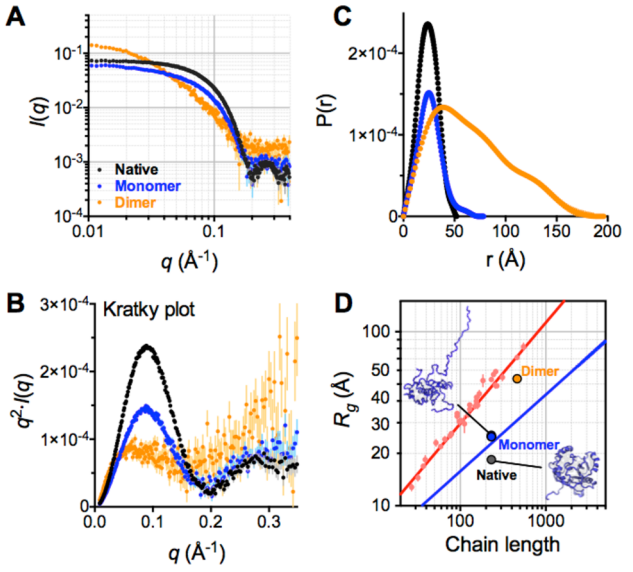

Figure 3. SAXS analyses for native and non-native forms of UCH-L1. (A) The SAXS profiles of the native state, monomeric, and dimeric folding intermediates at 2.7 M urea are colored in black, blue, and orange, respectively. (B) The Kratky plots transformed from the SAXS profiles. (C) The pair-wised distance distributions derive from the SAXS profiles using GNOM within the ATSAS software suite.[27] (D) R_g values of UCH-L1 in their native and urea-denatured folding intermediate states as a function of chain length. The red line and blue line are the empirical Flory's power law for chemically denatured proteins and for native proteins, respectively.[17]

contributions originated from the different oligomeric states (Figure 3A).

SAXS data were collected from well-separated SEC elution peaks corresponding to the native UCH-L1 without urea, and the monomeric and dimeric of UCH-L1 in the presence of 2.5, 2.7, and 3.0 M urea (gray shades in Figure S5A). The SEC-SAXS elution peak of the tetrameric folding intermediate of UCH-L1 was weak and overlapped with that of the dimeric intermediate in the presence of high urea concentration, which prevented further quantitative analyses (Figure S5A). For native, monomeric UCH-L1, the SAXS profile showed good agreement with the back-calculated SAXS profile based on the reported crystal structure of UCH-L1; the scattering contributions of the flexible hexahistidine tag at the C-terminus were included by using AllosMod-FoXS (Figure S5A and S6A).[28,29]

For the monomeric folding intermediate of UCH-L1, a significant reduction in the peak height of the Kratky plot was observed compared to that of the native profile (Figure 3B), indicating that the monomeric folding intermediate is partially unfolded. This is corroborated by the pairwise distance distribution, $P(r)$ (Figure 3C) and the increase radius of gyration (R_g) from 17.9 to 29.3 Å, derived from Guinier approximation (Figures 3D and S6). In order to characterize this partially unfolded intermediate, we performed molecular dynamics simulations to generate an ensemble of structures that collectively match the experimental SAXS profile collected in the presence of 3.3 M urea (Figure S6). Considering that a stable core structure encompassing the central β-sheet and α-helix 2 of UCH-L1 was observed in our earlier pulsed-labeling NMR HDX analysis,[21] the structural protections were used as restrains during the ensemble modeling (Supporting Information). A subset of conformations that closely resemble the monomeric folding intermediate was selected and the results showed partially unfolded peripheral helices and extended termini (inset in Figure 3D and Figure S6). Despite the partial unfolding, the monomeric folding intermediate of UCH-L1 is relatively compact according to its R_g value in comparison with other native proteins (Figure 3D).[30,31] Due to the lack of independent local structural information regarding the dimeric folding intermediate, we did not apply the same modeling procedure to obtain a structural ensemble. Nonetheless, the corresponding Kratky plot, $P(r)$ and R_g value (Figures 3) all indicated the presence of a highly disordered structure that adopts an expanded random coil-like ensemble. How such a disordered ensemble manages to form a well-defined dimer remains to be established. To the best of our knowledge, our findings represent the first example of defined sequential and reversible oligomerization events of chemically induced folding intermediates starting from a monomeric native state.

In this work, we identified by SEC-MALS the formation of well-defined UCH-L1 dimers and tetramers under non-native conditions (Figure 1). The oligomerization process of UCH-L1 WT was fully reversible upon removal of urea. Prolonged incubation of the PD-associated I93M variant, however, lead to irreversible precipitation when incubated with moderate amounts of urea, indicating that UCH-L1 is metastable and that the I93M mutation could tip the balance of proteostasis toward aggregation, causing cellular stress. Furthermore, SEC-SAXS and restrained molecular modeling revealed a less compact monomeric folding intermediate compared to the native monomer, and that partially unfolded UCH-L1 can assemble into specific dimer and subsequently into tetramer. Our current findings highlighted the intrinsic shortcoming of

DOI: 10.1021/acs.jpclett.8b00815
J. Phys. Chem. Lett. 2018, 9, 2433−2437

intrinsic fluorescence and far-UV circular dichroism that are insensitive to changes in the oligomeric state of UCH-L1. The folding pathways of UCH-L1 therefore need to be revised in light of our current findings.

We recently reported that UCH-L1 exhibits highly populated PUFs under native conditions, which share common structural features with urea-induced folding intermediates.[21] It is conceivable that UCH-L1 may dimerize under native conditions despite being sparsely populated. Indeed, dimerization of UCH-L1 under the native state has been reported to display unusual ubiquitin ligase activity.[31] Considering the geometry of ubiquitin binding site of UCH-L1, it would require substantial conformational rearrangements for the binding crevice to simultaneously accommodate two ubiquitin molecules by dimeric UCH-L1 for isopeptide bond formation. In summary, our findings echoed the notion of the fine balance between cellular protein abundance and solubility in proteostasis, as UCH-L1 is highly expressed in neuronal cells with the ability to transiently populate oligomeric states with considerable conformational disorder.[21] Structural perturbation and destabilization by the PD-associated I93M mutation could lead to irreversible precipitation when its folding intermediates are significantly populated and perturbed, which may occur under physiological conditions with elevated oxidative stress or aberrant proteostasis.[14]

■ ASSOCIATED CONTENT

Supporting Information

The Supporting Information is available free of charge on the ACS Publications website at DOI: 10.1021/acs.jpclett.8b00815.

Thermodynamics parameters derived from urea-induced equilibrium unfolding, chemical cross-linking, SEC-MALS/SAXS, and SAXS-based ensemble structural modeling results (PDF)

■ AUTHOR INFORMATION

Corresponding Author

*Tel +886-2-27855696 ext 5121; FAX: +886-2-27889759; E-mail: sthsu@gate.sinica.edu.tw.

ORCID

Shang-Te Danny Hsu: 0000-0002-7231-0185

Notes

The authors declare no competing financial interest.

■ ACKNOWLEDGMENTS

This work is supported by the Ministry of Science and Technology (MOST104-2113-M-001-016, MOST105-2113-M-001-005, and MOST 106-2113-M-001-004) and Academia Sinica, Taiwan. S.-T.D.H. is a recipient of the Career Development Award (CDA-00025/2010-C) from the International Human Frontier Science Program. We are grateful to the staff of BL23A1 of the National Synchrotron Radiation Research Center (NSRRC, Taiwan) for their expert assistance in SAXS data collection.

■ REFERENCES

(1) Chiti, F.; Dobson, C. M. Protein Misfolding, Functional Amyloid, and Human Disease. *Annu. Rev. Biochem.* **2006**, *75*, 333−366.

(2) Knowles, T. P.; Vendruscolo, M.; Dobson, C. M. The Amyloid State and Its Association with Protein Misfolding Diseases. *Nat. Rev. Mol. Cell Biol.* **2014**, *15*, 384−396.

(3) Breydo, L.; Uversky, V. N. Structural, Morphological, and Functional Diversity of Amyloid Oligomers. *FEBS Lett.* **2015**, *589*, 2640−2648.

(4) Buell, A. K.; Galvagnion, C.; Gaspar, R.; Sparr, E.; Vendruscolo, M.; Knowles, T. P.; Linse, S.; Dobson, C. M. Solution Conditions Determine the Relative Importance of Nucleation and Growth Processes in α-Synuclein Aggregation. *Proc. Natl. Acad. Sci. U. S. A.* **2014**, *111*, 7671−7676.

(5) Meisl, G.; Yang, X.; Hellstrand, E.; Frohm, B.; Kirkegaard, J. B.; Cohen, S. I.; Dobson, C. M.; Linse, S.; Knowles, T. P. Differences in Nucleation Behavior Underlie the Contrasting Aggregation Kinetics of the Aβ40 and Aβ42 Peptides. *Proc. Natl. Acad. Sci. U. S. A.* **2014**, *111*, 9384−9389.

(6) Cremades, N.; Cohen, S. I.; Deas, E.; Abramov, A. Y.; Chen, A. Y.; Orte, A.; Sandal, M.; Clarke, R. W.; Dunne, P.; Aprile, F. A.; et al. Direct Observation of the Interconversion of Normal and Toxic Forms of α-Synuclein. *Cell* **2012**, *149*, 1048−1059.

(7) Xue, W. F.; Homans, S. W.; Radford, S. E. Systematic Analysis of Nucleation-Dependent Polymerization Reveals New Insights into the Mechanism of Amyloid Self-Assembly. *Proc. Natl. Acad. Sci. U. S. A.* **2008**, *105*, 8926−8931.

(8) Orte, A.; Birkett, N. R.; Clarke, R. W.; Devlin, G. L.; Dobson, C. M.; Klenerman, D. Direct Characterization of Amyloidogenic Oligomers by Single-Molecule Fluorescence. *Proc. Natl. Acad. Sci. U. S. A.* **2008**, *105*, 14424−14429.

(9) Narayan, P.; Orte, A.; Clarke, R. W.; Bolognesi, B.; Hook, S.; Ganzinger, K. A.; Meehan, S.; Wilson, M. R.; Dobson, C. M.; Klenerman, D. The Extracellular Chaperone Clusterin Sequesters Oligomeric Forms of the Amyloid-β(1−40) Peptide. *Nat. Struct. Mol. Biol.* **2012**, *19*, 79−83.

(10) Wilkinson, K. D.; Lee, K. M.; Deshpande, S.; Duerksen-Hughes, P.; Boss, J. M.; Pohl, J. The Neuron-Specific Protein PGP 9.5 Is a Ubiquitin Carboxyl-Terminal Hydrolase. *Science* **1989**, *246*, 670−673.

(11) Leroy, E.; Boyer, R.; Auburger, G.; Leube, B.; Ulm, G.; Mezey, E.; Harta, G.; Brownstein, M. J.; Jonnalagada, S.; Chernova, T.; et al. The Ubiquitin Pathway in Parkinson's Disease. *Nature* **1998**, *395*, 451−452.

(12) Ardley, H. C.; Scott, G. B.; Rose, S. A.; Tan, N. G.; Robinson, P. A. UCH-L1 Aggresome Formation in Response to Proteasome Impairment Indicates a Role in Inclusion Formation in Parkinson's Disease. *J. Neurochem.* **2004**, *90*, 379−391.

(13) Kabuta, T.; Furuta, A.; Aoki, S.; Furuta, K.; Wada, K. Aberrant Interaction between Parkinson Disease-Associated Mutant UCH-L1 and the Lysosomal Receptor for Chaperone-Mediated Autophagy. *J. Biol. Chem.* **2008**, *283*, 23731−23738.

(14) Kabuta, T.; Setsuie, R.; Mitsui, T.; Kinugawa, A.; Sakurai, M.; Aoki, S.; Uchida, K.; Wada, K. Aberrant Molecular Properties Shared by Familial Parkinson's Disease-Associated Mutant UCH-L1 and Carbonyl-Modified UCH-L1. *Hum. Mol. Genet.* **2008**, *17*, 1482−1496.

(15) Koharudin, L. M. I.; Liu, H.; Di Maio, R.; Kodali, R. B.; Graham, S. H.; Gronenborn, A. M. Cyclopentenone Prostaglandin-Induced Unfolding and Aggregation of the Parkinson Disease-Associated UCH-L1. *Proc. Natl. Acad. Sci. U. S. A.* **2010**, *107*, 6835−6840.

(16) Kumar, R.; Jangir, D. K.; Verma, G.; Shekhar, S.; Hanpude, P.; Kumar, S.; Kumari, R.; Singh, N.; Sarovar Bhavesh, N.; Ranjan Jana, N.; et al. S-Nitrosylation of UCHL1 Induces Its Structural Instability and Promotes α-Synuclein Aggregation. *Sci. Rep.* **2017**, *7*, 44558.

(17) Lee, Y. T.; Hsu, S.-T. D. Familial Mutations and Post-Translational Modifications of UCH-L1 in Parkinson's Disease and Neurodegenerative Disorders. *Curr. Protein Pept. Sci.* **2017**, *18*, 733−745.

(18) Andersson, F. I.; Werrell, E. F.; McMorran, L.; Crone, W. J. K.; Das, C.; Hsu, S.-T. D.; Jackson, S. E. The Effect of Parkinson's-Disease-Associated Mutations on the Deubiquitinating Enzyme UCH-L1. *J. Mol. Biol.* **2011**, *407*, 261−272.

(19) Das, C.; Hoang, Q. Q.; Kreinbring, C. A.; Luchansky, S. J.; Meray, R. K.; Ray, S. S.; Lansbury, P. T.; Ringe, D.; Petsko, G. A. Structural Basis for Conformational Plasticity of the Parkinson's

DOI: 10.1021/acs.jpclett.8b00815
J. Phys. Chem. Lett. 2018, 9, 2433−2437

Disease-Associated Ubiquitin Hydrolase UCH-L1. *Proc. Natl. Acad. Sci. U. S. A.* **2006**, *103*, 4675−4680.
(20) Boudreaux, D. A.; Maiti, T. K.; Davies, C. W.; Das, C. Ubiquitin Vinyl Methyl Ester Binding Orients the Misaligned Active Site of the Ubiquitin Hydrolase UCHL1 into Productive Conformation. *Proc. Natl. Acad. Sci. U. S. A.* **2010**, *107*, 9117−9122.
(21) Lou, S. C.; Wetzel, S.; Zhang, H. Y.; Crone, E. W.; Lee, Y. T.; Jackson, S. E.; Hsu, S.-T. D. The Knotted Protein UCH-L1 Exhibits Partially Unfolded Forms under Native Conditions That Share Common Structural Features with Its Kinetic Folding Intermediates. *J. Mol. Biol.* **2016**, *428*, 2507−2520.
(22) Jeng, U. S.; Su, C. H.; Su, C. J.; Liao, K. F.; Chuang, W. T.; Lai, Y. H.; Chang, J. W.; Chen, Y. J.; Huang, Y. S.; Lee, M. T.; et al. A Small/Wide-Angle X-Ray Scattering Instrument for Structural Characterization of Air-Liquid Interfaces, Thin Films and Bulk Specimens. *J. Appl. Crystallogr.* **2010**, *43*, 110−121.
(23) Yeh, Y. Q.; Liao, K. F.; Shih, O.; Shiu, Y. J.; Wu, W. R.; Su, C. J.; Lin, P. C.; Jeng, U. S. Probing the Acid-Induced Packing Structure Changes of the Molten Globule Domains of a Protein near Equilibrium Unfolding. *J. Phys. Chem. Lett.* **2017**, *8*, 470−477.
(24) Shih, O.; Yeh, Y. Q.; Liao, K. F.; Sung, T. C.; Chiang, Y. W.; Jeng, U. S. Oligomerization Process of Bcl-2 Associated X Protein Revealed from Intermediate Structures in Solution. *Phys. Chem. Chem. Phys.* **2017**, *19*, 7947−7954.
(25) Shiu, Y. J.; Jeng, U. S.; Huang, Y. S.; Lai, Y. H.; Lu, H. F.; Liang, C. T.; Hsu, I. J.; Su, C. H.; Su, C.; Chao, I.; et al. Global and Local Structural Changes of Cytochrome C and Lysozyme Characterized by a Multigroup Unfolding Process. *Biophys. J.* **2008**, *94*, 4828−4836.
(26) Franke, D.; Petoukhov, M. V.; Konarev, P. V.; Panjkovich, A.; Tuukkanen, A.; Mertens, H. D. T.; Kikhney, A. G.; Hajizadeh, N. R.; Franklin, J. M.; Jeffries, C. M.; et al. ATSAS 2.8: A Comprehensive Data Analysis Suite for Small-Angle Scattering from Macromolecular Solutions. *J. Appl. Crystallogr.* **2017**, *50*, 1212−1225.
(27) Schneidman-Duhovny, D.; Hammel, M.; Sali, A. Foxs: A Web Server for Rapid Computation and Fitting of SAXS Profiles. *Nucleic Acids Res.* **2010**, *38*, W540−W544.
(28) Weinkam, P.; Pons, J.; Sali, A. Structure-Based Model of Allostery Predicts Coupling between Distant Sites. *Proc. Natl. Acad. Sci. U. S. A.* **2012**, *109*, 4875−4880.
(29) Kohn, J. E.; Millett, I. S.; Jacob, J.; Zagrovic, B.; Dillon, T. M.; Cingel, N.; Dothager, R. S.; Seifert, S.; Thiyagarajan, P.; Sosnick, T. R.; et al. Random-Coil Behavior and the Dimensions of Chemically Unfolded Proteins. *Proc. Natl. Acad. Sci. U. S. A.* **2004**, *101*, 12491−12496.
(30) Shih, P. M.; Wang, I.; Lee, Y. T.; Hsieh, S. J.; Chen, S. Y.; Wang, L. W.; Huang, C. T.; Chien, C. T.; Chang, C. Y.; Hsu, S.-T. D. Random-Coil Behavior of Chemically Denatured Topologically Knotted Proteins Revealed by Small-Angle X-Ray Scattering. *J. Phys. Chem. B* **2015**, *119*, 5437−5443.
(31) Liu, Y. C.; Fallon, L.; Lashuel, H. A.; Liu, Z. H.; Lansbury, P. T. The UCH-L1 Gene Encodes Two Opposing Enzymatic Activities That Affect α-Synuclein Degradation and Parkinson's Disease Susceptibility. *Cell* **2002**, *111*, 209−218.

DOI: 10.1021/acs.jpclett.8b00815
J. Phys. Chem. Lett. 2018, 9, 2433−2437